Journal of Molecular Structure 1011 (2012) 81–93

Contents lists available at SciVerse ScienceDirect

Journal of Molecular Structure

journal homepage: www.elsevier.com/locate/molstruc

Structural influences on the oxidation of a series of 2-benzothiazoline analogs

Matthew A. Lynn [a], Lauren J. Carlson [b], Hyeon Hwangbo [b], Joseph M. Tanski [c], Laurie A. Tyler [b,*]

[a] Department of Science and Mathematics, National Technical Institute for the Deaf, Rochester Institute of Technology, Rochester, NY 14623, United States
[b] Department of Chemistry and Biochemistry, Union College, Schenectady, NY 12308, United States
[c] Department of Chemistry, Vassar College, Poughkeepsie, NY 12604, United States

ARTICLE INFO

Article history:
Received 17 October 2011
Received in revised form 2 December 2011
Accepted 2 December 2011
Available online 17 December 2011

Keywords:
Benzothiazoline
Benzothiazole
Imine
Oxidation
Density functional calculations

ABSTRACT

We have examined the molecular and electronic structures of a number of benzothiazoline (Bt) and benzothiazole (oBt) analogs that possess phenyl and heterocycle substituents at the 2-position and discuss the ground-state factors that influence the relative rates at which these benzothiazolines are oxidized to benzothiazoles. Our studies indicate that the substituent at the 2-position in the benzothiazoline plays a fundamental role in governing the susceptibility of the species to oxidize. Our calculations for this series of compounds suggest that benzothiazolines that possess a heterocyclic R group oxidize faster than those with a phenyl group. The establishment of a favorable electrostatic interaction between the heteroatoms of the R and Bt/oBt fragments is a primary influence on this reaction while the establishment of π conjugation across the C_R—C_{oBt} bond is a minor effect.

1. Introduction

In the last few years we and others have focused research efforts on the synthesis, characterization, and study of heterocyclic thiazoline-based molecules [1–3]. Unlike their oxygen-containing counterparts, the oxazolines, thiazoline-based molecules have been studied less and we are finding that they can exhibit unique reactivity due to the sulfur atom. The thiazoline class of molecules has proven useful in the preparation of a diverse range of organic and inorganic systems. Indeed thiazolines can be used to prepare a variety of organic functional groups including thiazoles, β-amino thiols, aldehydes, and ketones to name a few [4,5]. Additionally, numerous coordination complexes have been obtained by starting with thiazoline-containing ligands. Some of these systems exhibit unique reactivity as well as electrochemical and photophysical properties and some have been employed as small molecule mimics for metalloproteins and enzymes [6–8].

It has been well documented in the field of inorganic chemistry that the thiazoline group opens in the presence of base or metal ion to form the corresponding imine (Scheme 1) [9,10]. As such, the cyclized thiazoline precursor gives this class of molecules an inherent advantage as ligands, not only by providing *N*-, *S*-coordination donors, but also inhibiting unwanted thiol oxidation.

A number of syntheses have been developed to obtain thiazoline-based molecules [4,5] and 2-benzothiazoline (Bt) analogs can be prepared by using a straightforward condensation reaction with *o*-aminobenzenethiol (ABT) and an aldehyde group. Although literature reports indicate that this reaction proceeds unencumbered [11,12], we experienced difficulties when carrying out reactions in our lab. Parallel syntheses utilizing ABT with various heterocyclic-substituted aldehydes resulted in the formation of both the expected 2-thiazoline product as well as another product that we identified as the oxidized, 2-benzothiazole (oBt) derivative (Scheme 2).

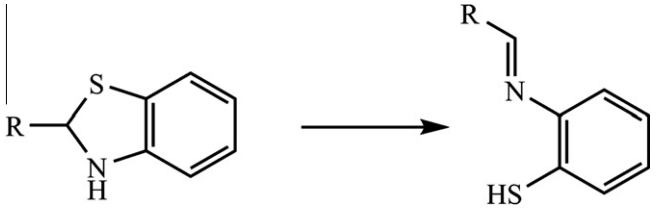

Scheme 1. Imine formation from a substituted 2-benzothiazoline molecule.

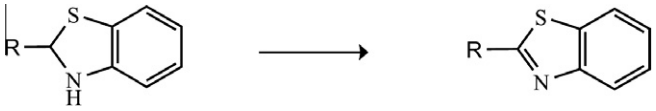

Scheme 2. Oxidation of a 2-benzothiazoline to a 2-benzothiazole.

Several synthetic methods employing different oxidative techniques have been reported for the conversion of a benzothiazoline to a benzothiazole (MnO_2 in benzene, $BrCCl_3$/DBU) [13–15] and

* Corresponding author. Tel.: +1 518 388 7123.
E-mail address: tylerl@union.edu (L.A. Tyler).

0022-2860/$ - see front matter © 2011 Elsevier B.V. All rights reserved.
doi:10.1016/j.molstruc.2011.12.001

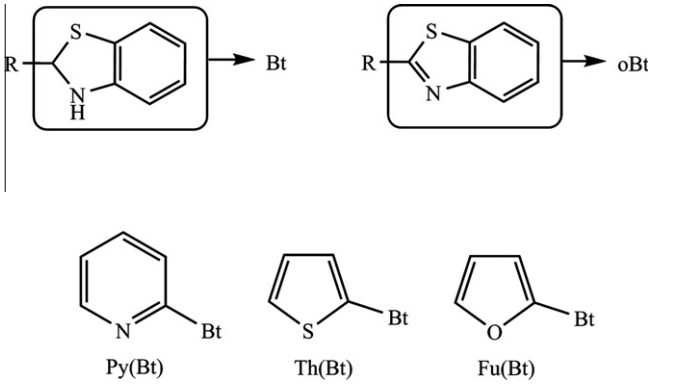

Fig. 1. Abbreviations employed in this work (top) and representative examples of benzothiazoline systems (bottom).

some reports also indicate oxygen can be used [16,17] however little mention of oxidation was noted in previous reports for the benzothiazoline species under reaction conditions similar to ours. Upon further investigation into the literature, we noted a curious lack of spectroscopic data for some of the heterocycle-substituted 2-benzothiazoline (Bt) analogs. It also appeared that ligation reactions with these analogs were problematic and many of the complexes were incompletely characterized [11,18–20,12,21]. As such, we were interested in acquiring the spectroscopic characterization for a set of substituted 2-benzothiazoline molecules useful in inorganic synthesis as well as their oxidized derivatives, the 2-benzothiazoles (oBt), in order to provide a spectral comparison [3]. The set included the pyridinyl- (Py-), thiophenyl- (Th-), and furanyl- (Fu-) substituted heterocyclic 2-benzothiazolines and 2-benzothiazoles shown in Fig. 1 (bottom). The acronym for each species was systematically assigned using an abbreviated form of the starting aldehyde (R) followed by (Bt) or (oBt) to differentiate between the thiazoline and the oxidized thiazole forms of the molecules respectively (see Fig. 1, top).

During the synthesis and characterization of this series of molecules, it became apparent that the substituent at the 2-position plays a fundamental role in governing the susceptibility toward oxidation of the 2-benzothiazolines. Therefore, as a follow up to our initial work, we have undertaken additional studies aimed at elucidating the structural and electronic factors responsible for the observed reactivity differences within this series of 2-thiazoline molecules by analyzing the ground state energetics of the set. This report, therefore, is directed toward defining the correlation between the substituent at the 2-postion in the benzothiazoline analog and the molecule's propensity to undergo oxidation to the corresponding 2-thiazole. We have also expanded the set by synthesizing four additional benzothiazoline analogs, shown in Fig. 2, in order to afford a more comprehensive comparison.

2. Experimental

2.1. Materials

2-Aminothiophenol, benzaldehyde, 4-methoxybenzaldehyde, 2-pyrrolecarboxaldehyde, and α,α,α-trifluoro-*p*-tolualdehyde were purchased from Aldrich Chemical Co. and used without further purification. All solvents and chemicals were of reagent grade and used without further purification.

2.2. Physical measurements

Infrared spectra were obtained with a Thermoelectron, Avatar 330 FT-IR spectrophotometer equipped with a Smart Orbit reflectance insert, diamond window. ^{1}H NMR spectra were recorded on a Varian 200 MHz spectrometer or on a Brüker 400 MHz spectrometer.

2.3. Preparation of the benzothiazoline and benzothiazole analogs

The new 2-benzothiazoline analogs, Ph(Bt), CF_3Ph(Bt), MeOPh(Bt) and Pyr(Bt), as well as those that were already known were synthesized following a procedure similar to one that we have previously published [3]. In each case 1 equiv of a substituted aldehyde was dissolved in ~20 mL of degassed ethanol (EtOH) to which was then added 1 equiv of neat ABT under an N_2 atmosphere. The reaction was then refluxed for 2 h after which the solvent was immediately removed in *vacuo*. The thiazoline product precipitated from the solution as the volume was reduced in all cases except Pyr(Bt). This reaction resulted in the formation of an oil which could be solidified after trituration with diethyl ether (Et_2O). The solids were collected and dried under vacuum for ~12 h. Yields for the analogs ranged from 40% to 80%. In all cases great care was taken to minimize exposure to oxygen.

The complete oxidation of the benzothiazolines to the corresponding benzothiazoles was achieved by vigorously stirring a solution of the analog dissolved in $CHCl_3$ in an open flask for ~5 h at room temperature. The solvent was then removed via rotary evaporation and the residue dried under high vacuum for 10 h. Yields of the benzothiazoles were quantitative.

The spectroscopic data for the four new analogs and the oxidized derivatives of each follows.

2.4. Characterization of the analogs

2.4.1. Benzothiazoline derivatives

2.4.1.1. 2-Phenylbenzothiazoline (Ph(Bt)). White solid, mp 69–71 °C. ^{1}H NMR ($CDCl_3$, 200 MHz, 25 °C, δ from TMS): 4.36 (s, 1H, NH), 6.38 (d, 1H), 6.72 (m, 2H), 6.99 (m, 2H), 7.34 (m, 3H), 7.55 (m, 2H). Selected IR bands: (cm^{-1}) 3386 (m), 1579 (m), 1470 (s), 1260 (m), 743 (s), 695 (s).

2.4.1.2. 2-(p-Methoxyphenyl)benzothiazoline (MeOPh(Bt)). White solid, mp 61–63 °C. 1H NMR ($CDCl_3$, 400 MHz, 25 °C, δ from TMS): 3.80 (s, 3H, CH_3), 4.32 (s, 1H, NH), 6.38 (d, 1H), 6.65 (d, 1H), 6.77 (t, 1H), 6.92 (m, 3H), 7.06 (d, 1H), 7.50 (d, 2H). Selected IR bands: (cm^{-1}) 1608 (m), 1578 (m), 1462 (m), 1247 (m), 1030 (m), 830 (m), 739(s).

2.4.1.3. 2-(p-Trifluoromethylphenyl)benzothiazoline (CF_3Ph (Bt)). White solid, mp 106–108 °C. 1H NMR ($CDCl_3$, 200 MHz, 25 °C, δ from TMS): 4.45 (s, 1H, NH), 6.42 (d, 1H), 6.77 (m, 2H), 7.03 (m,

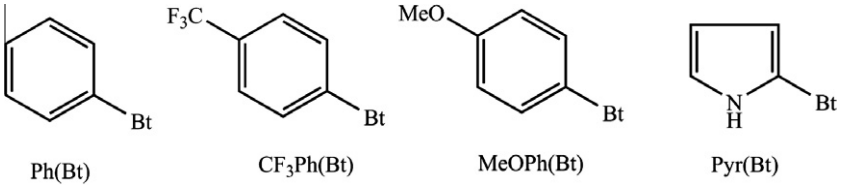

Fig. 2. Phenyl-(Ph-), *p*-trifluoromethylphenyl-(CF_3Ph-), *p*-methoxyphenyl (MeOPh-), and pyrrolyl-substituted (Pyr-) benzothiazoline analogs prepared as part of this study.

2H), 7.65 (d, 4H). Selected IR bands: (cm^{-1}) 1583 (m), 1475 (m), 1120 (m), 1106 (m), 1065 (s), 748 (s), 641 (s).

2.4.1.4. 2-Pyrrolylbenzothiazoline (Pyr(Bt)). Brown oil. ^1H NMR ($CDCl_3$, 400 MHz, 25 °C, δ from TMS): 4.36 (s, 1H, NH), 6.17 (m, 1H), 6.24 (s, 1H), 6.50 (s, 1H), 6.64 (d, 2H), 6.81 (m, 2H), 6.98 (t, 1H), 7.08 (d, 1H), 8.74 (s, 1H). Selected IR bands: (cm^{-1}) 1567 (m), 1485 (m), 1438 (m), 1397 (m), 1102 (m), 1039 (m), 1018 (m), 911 (m), 739(s). Selected IR bands: (cm^{-1}) 1580 (m, $\upsilon_{N=C}$), 1473(m), 975 (m), 743 (s).

2.4.2. Benzothiazole derivatives

2.4.2.1. 2-Phenylbenzothiazole (Ph(oBt)). Beige solid, mp 103 °C. 1H NMR ($CDCl_3$, 400 MHz, 25 °C, δ from TMS): 7.42 (t, 1H), 7.53 (m, 3H), 7.93 (d, 1H), 8.13 (m, 3H). Selected IR bands: (cm^{-1}) 3386 (m), 1579 (m, $\upsilon_{N=C}$), 1470 (s), 1260 (m), 743 (s), 695 (s).

2.4.2.2. 2-(p-Methoxyphenyl)benzothiazole (MeOPh(oBt)). White solid, mp 121–123 °C. 1H NMR ($CDCl_3$, 400 MHz, 25 °C, δ from TMS): 3.91 (s, 3H, CH_3), 7.03 (d, 2H), 7.38 (t, 1H),7.49 (t, 1H), 7.90 (d, 1H), 8.06 (d, 3H). Selected IR bands: (cm^{-1}) 1604 (m, $\upsilon_{N=C}$), 1483 (m), 1309 (m), 1254 (s) 1171 (s), 1026 (m), 967 (s), 831 (s), 757 (s).

2.4.2.3. 2-(p-Trifluoromethylphenyl)benzothiazole (CF_3Ph(oBt)). Yellow solid, mp 159–161 °C. ^1H NMR ($CDCl_3$, 400 MHz, 25 °C, δ from TMS): 7.46 (t, 1H), 7.56 (t, 1H), 7.78 (d, 2H), 7.96 (d, 1H), 8.13 (d, 1H), 8.23 (d, 2H). Selected IR bands: (cm^{-1}) 1585 (m, $\upsilon_{N=C}$), 1456 (m), 1433 (s) 1317 (m), 996 (m), 980 (s), 758 (s), 739 (s), 728 (s).

2.4.2.4. 2-Pyrrolylbenzothiazoline (Pyr(oBt). Beige solid, mp 100 °C, decomp. ^1H NMR ($CDCl_3$, 400 MHz, 25 °C, δ from TMS): 6.35 (m, 1H), 6.88 (s, 1H), 7.00 (s, 1H), 7.33 (t, 1H), 7.46 (t, 1H), 7.86 (d, 1H), 7.92 (d, 1H), 9.94 (s, 1H). Selected IR bands: (cm^{-1}) 3119 (w), 1570 (m, $\upsilon_{N=C}$), 1486 (s), 1438 (s), 1397 (s), 1136 (m), 1040 (m), 912 (s), 740 (s).

2.5. X-ray data collection and structure solution and refinement

Single crystals suitable for X-ray analysis were obtained using the following procedures: Diffusion of Et_2O into separate chloroform solutions of Ph(Bt) and Py(Bt) resulted in the formation of yellow and colorless plates of each analog respectively within 24 h. Slow evaporation of separate solutions of Py(oBt) and Ph(oBt) resulted in the formation of colorless blocks of each species. X-ray diffraction data were collected on a Bruker APEX 2 CCD platform diffractometer (Mo Kα (λ = 0.71073 Å)) equipped with an Oxford liquid nitrogen cryostream. Crystals were mounted in a nylon loop with Paratone-N cryoprotectant oil. The structures were solved using direct methods and standard difference map techniques, and were refined by full-matrix least-squares procedures on F^2 with SHELXTL (Version 6.14) [22]. All non-hydrogen atoms were refined anisotropically. Hydrogen atoms on carbon were included in calculated positions and were refined using a riding model. Crystal data and refinement details are presented in Table 1 for all species while selected bond distances and angles are listed in Table 2 and Table 3 respectively.

2.6. Computational details

All calculations were performed using the Intel Macintosh version of Gaussian 03, Revision E.01 [23]. The gas-phase equilibrium geometries of the benzothiazolines and benzothiazoles were optimized by the hybrid density functional B3LYP method [24–26]. The 6-31G(*d*) basis set was used as supplied with the software. This combination of functional and basis set was chosen because of its ability to generate molecular structures that agreed well with our experimentally obtained crystal structures of various benzothiazoline and benzothiazole systems at reasonable computational expense. All stationary points were identified as local minima through the use of vibrational analysis.

3. Results and discussion

3.1. Synthesis and spectral characterization

Oxidation of the 2-benzothiazoline group has been observed since the 1930s when Lankelma and Sharnoff reported that benzothiazolines react in the process of purification [27]. Likewise, Yamamoto et al. have reported that 3-unsubstituted benzothiazoline derivatives are unstable in solution and also oxidize easily in air [28]. In both of these examples the authors noted that the benzothiazolines were oxidized to the corresponding benzothiazoles, resulting in the formation of a C=N double bond within the ring structure (Scheme 2). Although studies of N-alkylated benzothiazolines have indicated that they are susceptible toward oxidation, these compounds oxidize to generate products in which the five-membered ring has opened [29]. In line with these former reports, our own experience handling 2-benzothiazolines indicates that they are prone to react in air and that some analogs are more susceptible toward oxidation than others. As such, the preparations for the set of benzothiazoline molecules presented in this study were carried out to carefully exclude oxygen to avoid contamination with the oxidized benzothiazole and afford clean spectroscopic characterization of each. The corresponding benzothiazole analogs were isolated by vigorously stirring a chloroform solution of the benzothiazoline in air, with complete oxidation occurring after no more than 5 h. ^1H NMR spectroscopy was used to monitor the (Bt) → (oBt) transformation as well as to confirm the purity of each thiazoline and thiazole analog. Fig. 3 depicts the oxidation reaction for MeOPh(Bt), monitored by ^1H NMR spectroscopy ($CDCl_3$). The top spectrum of this figure shows clean MeOPh(Bt) while the completely oxidized product, MeOPh(oBt), is evident in the bottom spectrum.

Several pieces of spectroscopic information can be used to determine the degree to which the oxidation reaction has occurred. First, there are two distinct resonances present in the ^1H NMR spectrum of MeOPh(Bt) that can be used to identify the benzothiazoline group. One resonance, located between ~4.4 and 5.1 ppm, is assigned to the benzothiazoline N—H as confirmed by D_2O exchange. The other resonance, attributed to the thiazoline C—H proton, appears as a singlet between 6.3 and 6.7 ppm. The N—H peak can be broad which makes the thiazoline C—H resonance a better indicator for the presence of this species and a good gauge to determine the extent of oxidation. Additionally, ^1H NMR spectra show that as the benzothiazolines oxidize there is a concomitant downfield shift in the aromatic resonances, most likely due to the extended conjugation between the two ring systems upon oxidation. The second method includes analysis of the IR spectra for the (Bt) and (oBt) analogs which reveals only slight differences between the two forms, including the appearance of a medium intensity band ~1600 cm^{-1} that can be assigned to the thiazole $\upsilon_{C=N}$.

Although the benzothiazoline N—H bond clearly plays a role in the oxidation process, we have found that the propensity of a benzothiazoline to undergo oxidation to form the corresponding benzothiazole is also directly dependent on the molecular structure of the ring system bound to the 2-position. The relative rates of reactions occur in the following order for the set of seven analogs we have studied: Fu(Bt) ~ Pyr(Bt) > Thio(Bt) > Ph(Bt) > CF_3Ph(Bt) > MeOPh(Bt) > Py(Bt), from fastest to slowest. In order to obtain this

Table 1
Summary of crystal data and intensity collection and structure refinement parameters for thiazoline and thiazole analogs.

	Ph(Bt)	Py(Bt)	Ph(oBt)	Py(oBt)
Empirical formula	$C_{13}H_{11}NS$	$C_{12}H_{10}N_2S$	$C_{13}H_9NS$	$C_{12}H_8N_2S$
Molecular Weight	213.29	214.28	211.27	212.26
Crystal color, habit	Yellow, plate	Colorless, plate	Colorless, block	Colorless, block
Crystal size (mm)	0.33 × 0.14 × 0.04	0.15 × 0.05 × 0.01	0.27 × 0.10 × 0.08	0.23 × 0.13 × 0.13
Temperature (K)	125(2)	125(2)	125(2)	125(2)
Crystal System	Triclinic	Orthorhombic	Orthorhombic	Orthorhombic
Space group	P-1	P2(1)2(1)2(1)	Pna2(1)	Pca2(1)
Unit cell dimensions				
a (Å)	8.4439(1)	6.1793(6)	16.1330(1)	13.7445(6)
b (Å)	11.1521(2)	8.6385(9)	11.0617(9)	13.0249(6)
c (Å)	11.3664(2)	19.256(2)	5.7804(5)	11.0599(5)
α (°)	89.661(2)	90	90	90
β (°)	88.568(2)	90	90	90
γ (°)	87.174(2)	90	90	90
V (Å^3), Z	1068.7(3), 4	1027.90(2), 4	1031.56(2), 4	1979.95(2), 8
D_{calc} (mg m^{-3})	1.326	1.385	1.360	1.424
Absorption coeff. (μ, mm^{-1})	0.265	0.278	0.274	0.289
Φ Range collected (°)	1.79–28.33	2.12–24.72	2.23–24.75	1.56–29.13
Completeness to Φ max (%)	98.7	100	99.9	100
Reflns collected/unique ($R(int)$)	13829/5261 (0.0315)	10361/1761 (0.1008)	9840/1756 (0.0651)	26392/5320 (0.0323)
Data/restraints/parameters	5261/2/277	1761/1/139	1756/443/273	5320/1/272
R_1, wR_2 ($I > 2\sigma I$)	0.0602, 0.1599	0.0415, 0.0634	0.0299, 0.0593	0.0536, 0.1399
R_1, wR_2 (all data)	0.0807, 0.1750	0.0721, 0.0727	0.0345, 0.0606	0.0581, 0.1443
Goodness of fit on F^2	1.074	1.050	1.173	1.055
Largest diff peak/hole (e/Å^3)	1.041, −0.434	0.220, −0.228	0.091, −0.116	2.606, −0.498
Absolute structure parameter		0.51(1)	−0.11(9)	0.00(9)

Table 2
Selected bond distances (Å) for thiazoline and thiazole analogs determined by X-ray crystallography.

Ph(Bt)			
S(1)—C(11)	1.852(3)	C(11)—C(12)	1.513(3)
S(1)—C(18)	1.760(3)	C(11)—H(11A)	1.0000
C(11)—N(1)	1.451(3)	C(12)—C(17)	1.399(3)
N(1)—C(113)	1.387(3)	C(12)—C(13)	1.393(4)
N(1)—H(1)	0.878(2)	C(18)—C(113)	1.398(3)
S(2)—C(21)	1.847(3)	C(21)—C(22)	1.524(3)
S(2)—C(28)	1.767(3)	C(21)—H(21A)	1.0000
C(21)—N(2)	1.456(3)	C(22)—C(27)	1.391(3)
N(2)—C(213)	1.384(3)	C(22)—C(23)	1.392(4)
N(2)—H(2)	0.874(2)	C(28)—C(213)	1.405(3)
Py(Bt)			
S—C(1)	1.776(3)	C(1)—C(2)	1.501(4)
S—C(8)	1.841(3)	C(1)—H(1B)	1.0000
C(1)—N(1)	1.464(4)	C(2)—C(7)	1.383(4)
N(1)—C(13)	1.401(4)	N(2)—C(2)	1.349(3)
N(1)—H(1)	0.897(2)	C(8)—C(13)	1.393(4)
Ph(oBt)			
S—C(1)	1.749(4)	C(1)—C(2)	1.496(6)
S—C(8)	1.718(4)	C(2)—C(7)	1.378(6)
C(1)—N	1.297(5)	C(2)—C(3)	1.371(6)
N—C(13)	1.390(5)	C(8)—C(13)	1.389(5)
Py(oBt)			
S(11)—C(11)	1.747(3)	C(11)—C(12)	1.474(4)
S(11)—C(18)	1.750(3)	C(12)—C(17)	1.406(5)
C(11)—N(11)	1.300(4)	C(12)—N(12)	1.341(5)
N(11)—C(113)	1.392(4)	C(18)—C(113)	1.403(5)
S(21)—C(21)	1.751(3)	C(21)—C(22)	1.470(4)
S(21)—C(28)	1.742(3)	C(22)—C(27)	1.388(4)
C(21)—N(21)	1.305(3)	C(22)—N(22)	1.344(4)
N(21)—C(213)	1.389(3)	C(28)—C(213)	1.405(4)

Table 3
Selected bond angles (°) for thiazoline and thiazole analogs determined by X-ray crystallography.

Ph(Bt)			
C(18)—S(11)—C(11)	91.46(1)	N(1)—C(11)—C(12)	115.8(2)
C(11)—N(1)—C(113)	114.8(2)	N(1)—C(11)—S(1)	103.27(2)
C(17)—C(12)—C(11)	121.9(2)	C(13)—C(12)—C(17)	118.9(2)
C(11)—N(1)—H(1)	118.2(2)	N(2)—C(21)—C(22)	115.5(2)
C(28)—S(21)—C(21)	91.10(1)	N(2)—C(21)—S(2)	103.49(2)
C(21)—N(2)—C(213)	114.4(2)	C(23)—C(22)—C(27)	119.0(2)
C(27)—C(22)—C(21)	122.6(2)		
C(21)—N(2)—H(2)	122.2(2)		
Py(Bt)			
C(8)—S—C(1)	89.98(1)	N(1)—C(1)—C(2)	115.3(3)
C(1)—N(1)—C(13)	111.1(2)	N(1)—C(1)—S	103.78(2)
C(7)—C(2)—C(1)	123.4(3)	N(2)—C(2)—C(7)	122.8(3)
C(1)—N(1)—H(1)	111.8(2)		
Ph(oBt)			
C(8)—S—C(1)	88.5(2)	N—C(1)—C(2)	122.7(4)
C(1)—N—C(13)	110.3(4)	N—C(1)—S	116.0(3)
C(7)—C(2)—C(1)	119.8(5)	C(3)—C(2)—C(7)	120.4(5)
Py(oBt)			
C(18)—S(11)—C(11)	88.77(2)	N(11)—C(11)—C(12)	123.1(3)
C(11)—N(11)—C(113)	109.1(3)	N(11)—C(11)—S(11)	117.2(3)
C(7)—C(2)—C(1)	121.4(3)	N(12)—C(12)—C(17)	123.9(3)
C(28)—S(21)—C(21)	88.61(1)	N(21)—C(21)—C(22)	123.0(2)
C(21)—N(21)—C(213)	110.0(2)	N(21)—C(21)—S(21)	116.5(2)
C(27)—C(22)—C(21)	121.2(2)	N(22)—C(22)—C(27)	123.0(3)

ranking, studies using ^{1}H NMR spectroscopy were performed that followed the conversion of the benzothiazoline to thiazole over time.

In the following discussions, X-ray crystallographic analyses and detailed computational studies of the (Bt) and (oBt) analogs are presented to elucidate the structural and ground-state electronic factors responsible for the observed reactivity differences within this series of molecules.

3.2. Crystallographic structures of compounds

In order to provide a structural comparison between the thiazoline and thiazole forms of a molecule as well determine any structural differences that may be present between the different (Bt) and (oBt) moieties, X-ray crystallographic studies were carried out on Ph(Bt), Py(Bt), Ph(oBt) and Py(oBt). Although the syntheses for Py(Bt) and Py(oBt) have been reported previously [3], we report the structures here for the first time. For clarity

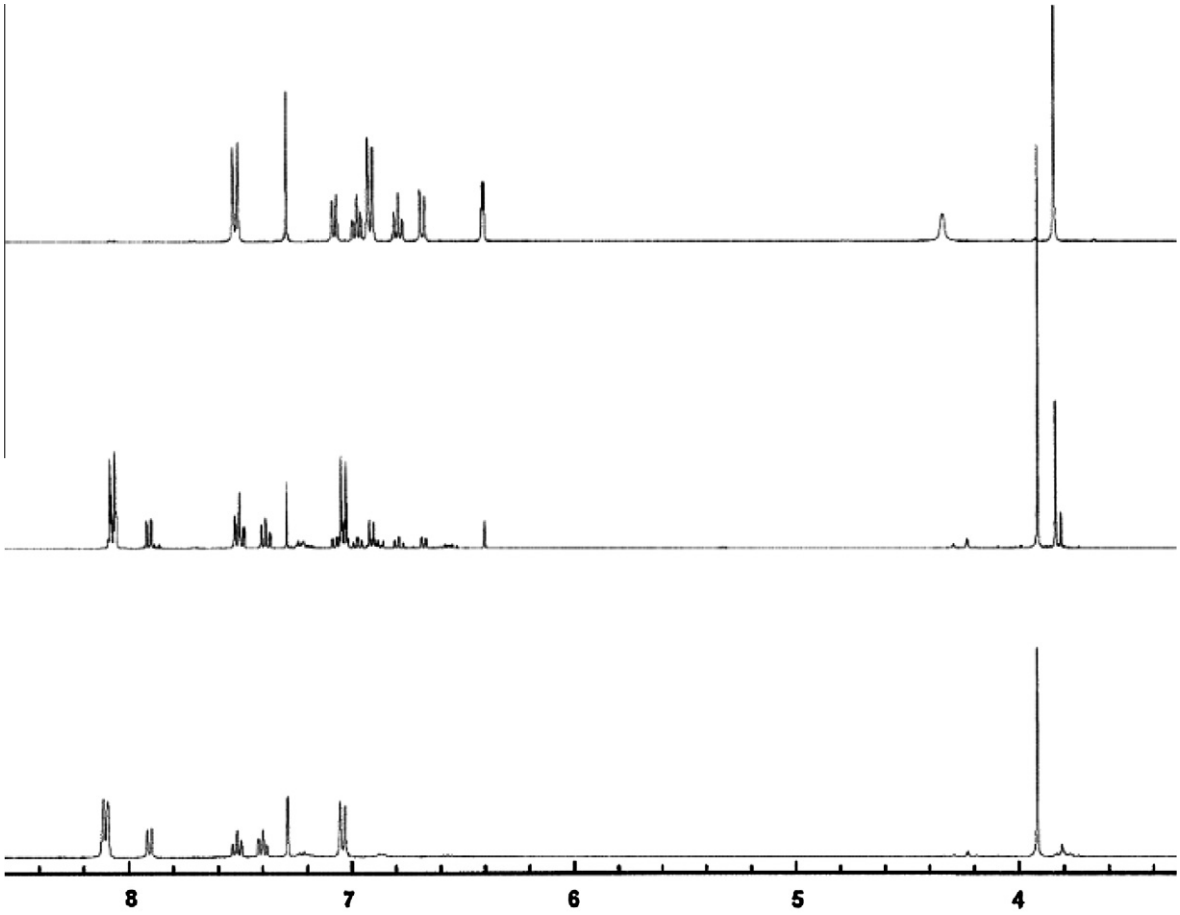

Fig. 3. Conversion of MeOPh(Bt) (top spectrum) to MeOPh(oBt) (bottom spectrum) over time followed by ^{1}H NMR spectroscopy ($CDCl_3$).

and ease of comparison, the numbering scheme between the four structures has been conserved.

3.2.1. Structures of Ph(Bt) and Py(Bt)

The X-ray analysis of Ph(Bt) revealed two independent molecules that in the asymmetric unit (Fig. 4). The highest difference peak of 1.041 e/Å^3 is found next to sulfur, the heavy atom in the structure. The bond lengths between the two molecules are similar, with differences less than 0.01 Å for analogous distances. The structure of Py(Bt) is shown in Fig. 5; this compound crystallizes as a racemic twin. While bond lengths for both sets of molecules are listed in Table 2, for discussion purposes the averages are used.

Comparison of the X-ray crystallographic data for Ph(Bt) and Py(Bt) reveals that the two structures are similar. The difference ~0.01 Å between the C(1)—C(2) bond lengths suggests that the bond order between these two atoms that join the thiazoline portion of the molecule and the substituent derived from the starting aldehyde is nearly equivalent between the two species. A

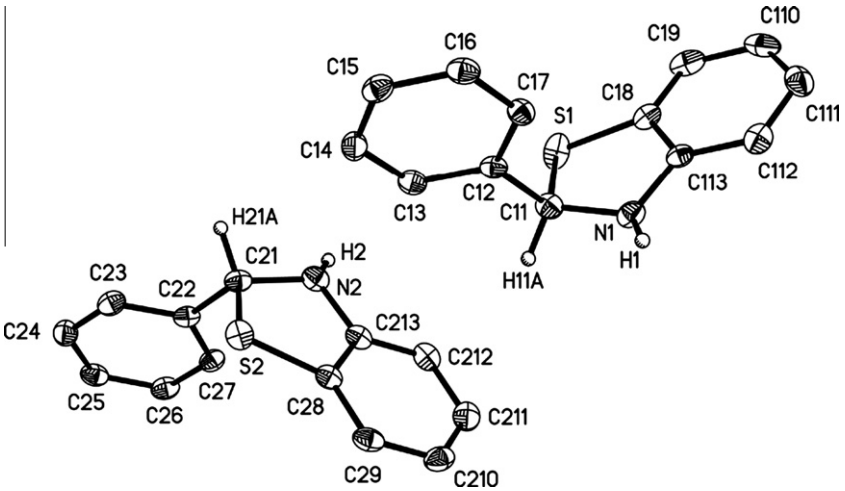

Fig. 4. Thermal ellipsoid plot (30% probability level) of Ph(Bt) showing the numbering scheme. Two independent molecules are in the unit cell.

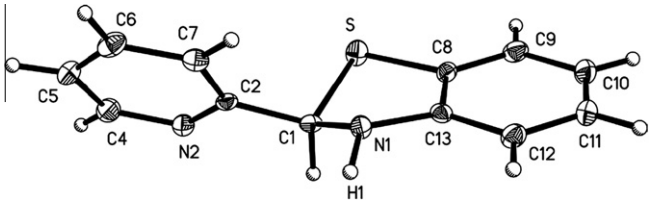

Fig. 5. Thermal ellipsoid plot (30% probability level) of Py(Bt) showing the numbering scheme.

comparable difference is noted in the C(1)—N(1) bond lengths within the thiazoline ring structure which measure 1.454(3) and 1.464(4) for Ph(Bt) and Py(Bt) respectively. There are however two main differences between these thiazoline analogs. The first in the C(1)—S bond lengths which measure 1.850(3) Å in Ph(Bt) and 1.776(3) Å in Py(Bt), a difference of ~0.07 Å. The other difference between the two structures is that Py(Bt) exhibits a one dimensional hydrogen-bonding chain between the N—H in the thiazoline portion of the molecule with the pyridine nitrogen of a neighboring molecule. The N1···N2$_i$ distance is 3.119(3) Å (symmetry codes: (i) $x + 1/2$, $-y1/2$, $-z + 1$). A structure showing this interaction is available in the Supplementary material. Ph(Bt) does not contain a heterocyclic substituent that can participate in H-bonding and no intermolecular hydrogen-bonding interaction occurs between the thiazoline nitrogen and thiazoline hydrogen of separate molecules.

3.2.2. Structures of Ph(oBt) and Py(oBt)

The structure of Ph(oBt) is shown in Fig. 6. The planar structure exhibits a twofold whole-molecule disorder that refined to 60/40 occupancy. A figure depicting this disorder is available in the Supplementary material. The disorder was refined with the help of similarity restraints on displacement parameters and rigid bond restraints on 1–2 and 1–3 distances and displacement parameters for all carbon atoms. The structure of Py(oBt) is shown in Fig. 7. Like Ph(Bt), Py(oBt) also crystallizes as two independent molecules in the asymmetric unit. The highest difference peak of 2.606 e/Å^3 is found next to the sulfur, the heavy atom in the structure. For both Ph(oBt) and Py(oBt), average bond lengths and angles will be used for the discussion while separate values are listed in Tables 2 and 3.

As expected, the C(1)—N(1) bond distances in both species decrease upon oxidation. These bond lengths for the two molecules are nearly identical ($\Delta \sim 0.006$ Å) and measure 1.297(3) and 1.303(3) Å for Ph(oBt) and Py(oBt) respectively. This structural change reflects a shortening of the C(1)—N(1) distances in going from (Bt) → (oBt) in both species by ~0.16 Å upon oxidation and represents the conversion of a C—N single bond into a C═N double bond. The C(1)—C(2) bond distance also decreases upon oxidation

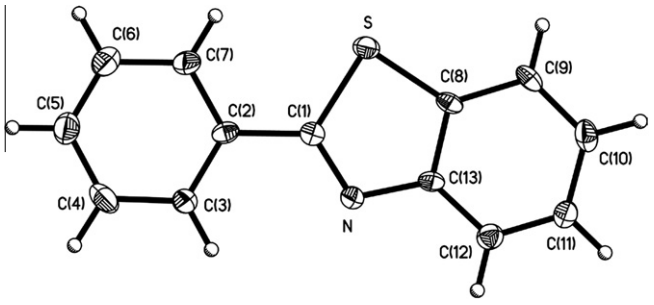

Fig. 6. Thermal ellipsoid plot (30% probability level) of Ph(oBt) showing the numbering scheme.

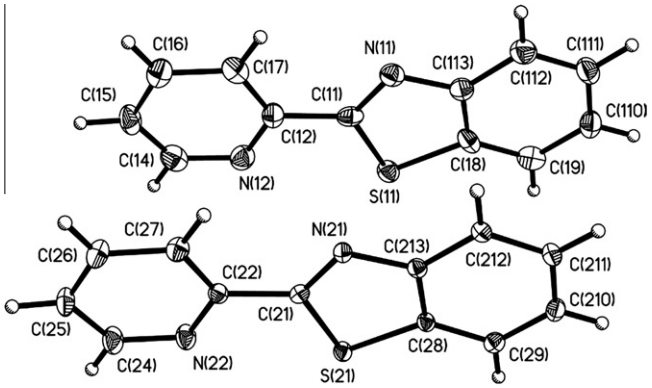

Fig. 7. Thermal ellipsoid plot (30% probability level) of both Py(oBt) molecules that cocrystallize within asymmetric unit. The numbering scheme is shown.

with similar lengths measured for Ph(oBt) and Py(oBt) (1.496(3) and 1.472(4) Å respectively). This change, however, is smaller than that for the C(1)—N(1) bond length upon oxidation. A difference of ~0.023 Å is noted for Ph(Bt) → Ph(oBt) while the analogous difference for the pyridine analog was found to be ~0.029 Å. Similarly, we observe that the C(1)—S bond lengths, which differed by ~0.07 Å between the Ph(Bt) and Py(Bt) analogs, become identical upon oxidation: 1.749(4) Å for Ph(oBt) and 1.749(3) Å for Py(oBt).

3.3. Computational analysis

3.3.1. Computational details of 2-benzothiazoline systems

An examination of the effect that a particular R group has on the oxidation of the various benzothiazoline systems prepared here first requires an understanding of the molecular structures of these compounds. Density functional theory, as implemented in the Gaussian 03 software package, was therefore employed to determine the optimized geometry of each R(Bt) molecule in the ground state. A ball-and-stick depiction of Ph(Bt), the structure for which is representative of most of the other R(Bt) systems, is shown at the top of Fig. 8. A number of atoms in this figure are labeled with subscripts that reference the portion of the molecule where they are located (e.g., N_{Bt}, the nitrogen atom in the benzothiazoline fragment; C_{oBt}, the carbon atom at the 2 position of the benzothiazole). Various optimized bond lengths, angles, and dihedral angles for these systems are provided in Table 4.

Comparison of the computationally optimized values in Table 4 with the crystallographically determined parameters in Tables 2 and 3 shows that the various optimized bond lengths and angles in the optimized structures compare well with the same parameters determined from the crystal structures. The C—C bond that bridges the Bt and R groups similarly falls within a narrow range of 1.483–1.511 Å. Furthermore, across the range of compounds, the H—C_{Bt}—C_R angle of approximately 109° is what would be expected for the tetrahedral carbon atom of the Bt unit (C_{Bt}). The values in parentheses in Table 4 show that the various optimized bond lengths and angles in the optimized structures compare well with the same parameters determined from the crystal structures.

Presented in Table 5 are the charges calculated for various atoms of the Bt unit and for the R group as a whole. It can be seen that these values vary little among this series of compounds and show no apparent trend from Py(Bt), which is oxidized the slowest, to Fu(Bt) and Pyr(Bt), which react the fastest. As was the case for the optimized bond lengths, angles, and dihedral angles presented in Table 4, the charges on the various atoms lie within narrow ranges and do not increase or decrease in a manner that correlates with the observed relative rates of reaction. In fact, the total charge

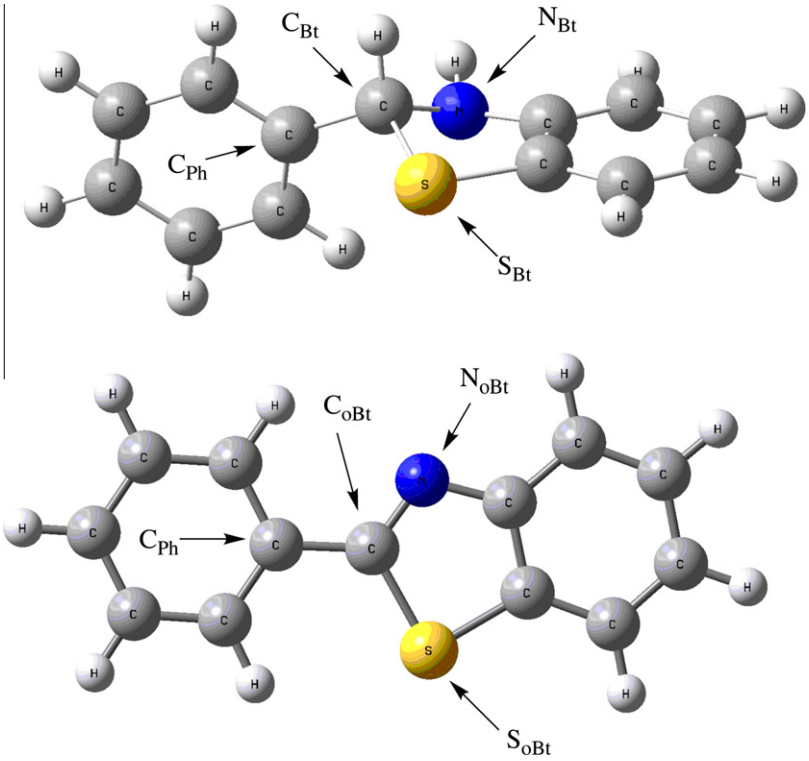

Fig. 8. DFT-optimized structures for Ph(Bt) and Ph(oBt) with atom-labeling scheme used herein.

Table 4
Structural parameters for the DFT-optimized ground-state structures of R(Bt). A positive dihedral angle indicates that the fourth atom (*E*) is rotated toward N_{Bt} while a negative angle means that it is rotated toward S_{Bt}.

R	S_{Bt}—C_{Bt} (Å)	N_{Bt}—C_{Bt} (Å)	C_{Bt}—C_R (Å)	H_{Bt}—C_{Bt}—C_R angle (°)	H_{Bt}—C_{Bt}—C_R—E'_R dihedral angle (°)
Ph	1.874	1.464	1.510	109.1	−15.3 (E = C_{Ph})
Py	1.861	1.463	1.536	108.2	97.5 (E = N_{Py})
CF_3Ph	1.873	1.463	1.511	109.1	−17.8 (E = C_{CF3Ph})
Th	1.880	1.464	1.491	108.2	−17.9 (E = C_{Th})
MeOPh	1.877	1.465	1.506	109.1	−13.6 (E = C_{MeOPh})
Fu	1.884	1.462	1.486	108.9	−28.0 (E = O_{Fu})
Pyr	1.886	1.471	1.483	108.9	−11.9 (E = C_{Pyr})

of the R fragment decreases from R = Ph to R = Th and then increases from R = Th to R = Pyr such that the total charge on the phenyl portion of Ph(Bt) (0.111) is similar to that for the pyrrolyl fragment of Pyr(Bt) (0.134). What does seem important, however, is the nature of the charge (either positive or negative) on several individual atoms in the Bt fragment. Our calculations determine that there is a positive charge in the range of +0.132 to +0.162 on S_{Bt} and a negative charge of −0.621 to −0.653 on N_{Bt}. As will be discussed shortly, this separation of charges within the Bt fragment itself plays an important role in the propensity of the R(Bt) systems to oxidize.

The one R(Bt) system for which Gaussian locates a ground-state structure that is different than the others is Py(Bt). Ball-and-stick representations of two perspectives of this molecule are shown in Fig. 9. Comparing this structure with that for Ph(Bt) (Fig. 8), the phenyl and pyridinyl rings are computed to be in orientations that are perpendicular to each other relative to the benzothiazoline fragments in the two molecules. The H_{Bt}—C_{Bt}—C_{Py}—N_{Py} dihedral angle between the Py and Bt portions of the molecule is 97.5°, considerably different than the approximately 15° calculated for the analogous angle in other R(Bt) systems. This differently configured lowest energy structure for Py(Bt) is found because of an electrostatic attraction between the positive charge

Table 5
Atomic charges for S_{Bt}, N_{Bt}, and C_{Bt} atoms in R(Bt) as well as the H atoms bound to the C and N atoms of the Bt fragment. Also shown is the total sum of atomic charges for each R group.

R	S_{Bt}	N_{Bt}	C_{Bt}	HC_{Bt}	HN_{Bt}	R
Ph	+0.153	−0.643	−0.204	+0.166	+0.319	+0.111
Py	+0.132	−0.621	−0.225	+0.197	+0.342	+0.079
CF_3Ph	+0.161	−0.645	−0.205	+0.170	+0.321	+0.088
Th	+0.162	−0.646	−0.177	+0.176	+0.324	+0.055
MeOPh	+0.148	−0.642	−0.205	+0.170	+0.321	+0.088
Fu	+0.159	−0.646	−0.212	+0.182	+0.322	+0.090
Pyr	+0.141	−0.653	−0.217	+0.175	+0.321	+0.134

(+0.342) on the H atom bound to N_{Bt} and the negative charge (−0.489) and available lone pair of electrons on N_{Py}. Similar computational [30,31] and experimental [32] findings have been made for substituted thiazolines and related systems with recent work [33] focusing on the effect of solvation on such compounds. This interaction provides for a slightly more stable molecular structure than if the Py ring were oriented similar to the R groups in other R(Bt) systems. It is also possible to locate a structure for Py(Bt) like those for the other R(Bt) systems in which the plane of the Py

fragment is approximately perpendicular to that of the Bt portion of the molecule, but this structure is 1.31 kcal/mol less stable than the one shown in Fig. 9.

If there is indeed such a long-range interaction between the lone pair of electrons on N_{Py} and H_{Bt} such that the lowest energy molecular structure for Py(Bt) is not like that shown in Fig. 8 for the phenyl-substituted benzothiazoline, it must be explained why similar structures are not found for the two other molecules that possess an R group having a heteroatom with an available σ-type lone pair of electrons, namely Fu(Bt) and Th(Bt). A structure for Fu(Bt) that is oriented like that shown in Fig. 9 can indeed be located, but the total energy of the structure is 0.46 kcal/mol less stable than the structure analogous to that shown in Fig. 9 even though the charge on the O atom is similar (−0.44) to that found for N_{Py}. The O_{Fu}—H_{Bt} distance in this furanyl system is 2.675 Å, which is 0.475 Å longer than the N_{Py}—H_{Bt} distance in Py(Bt). This difference between these two molecules is a result of two factors. First, the electron pair on the more electronegative O atom of Fu is less available than is the lone pair on the less electronegative N_{Py}. Second, the oxygen atom of the five-membered furanyl ring is farther away from the N_{Bt} H atom than is the nitrogen atom of the six-membered pyridinyl ring. As for Th(Bt), the charge calculated for S_{Th} is +0.28, so a long-range electrostatic attraction between it and the positively charged H atom bound to N_{Bt} does not occur.

3.3.2. Computational details of 2-benzothiazole systems and implications for oxidation

Upon oxidation, several important structural changes occur as R(Bt) becomes R(oBt). C_{Bt} and N_{Bt} gain p_π orbitals that can interact with the π system of the rest of the Bt fragment. Further, because all of the R groups being considered here possess their own π systems, each of the R(oBt) systems can have a conjugated π system that extends across the entire molecule when the R and oBt fragments are coplanar. Geometry optimizations of the various R(oBt) systems do indicate that the lowest energy structure for each molecule is indeed planar in agreement with the crystal structures (Figs. 6 and 7). A representative computed structure, that for (Ph(oBt)), is displayed at the bottom of Fig. 8.

One important aspect to understanding the structures of the R(oBt) systems is that some of them have a non-symmetric, heteroatom-containing R group. For R = Fu, Th, Py, and Pyr, the presence of the O, S, or N atom in the ring means that two different conformers can be generated depending on whether the heteroatom is located syn to N_{oBt} or to S_{oBt}. The differences in total energy between the two conformations for each of these molecules are: 1.46 kcal/mol (Th(oBt)), 2.16 kcal/mol (Fu(oBt)), 3.46 kcal/mol (Pyr(oBt)), and 6.72 kcal/mol (Py(oBt)). The orientation with the lower energy for Py(oBt) has the N_{py} atom syn to S_{oBt} in agreement with this compound's crystal structure (Fig. 7). Similarly, our calculations find that the lower energy planar structure for Fu(oBt) has

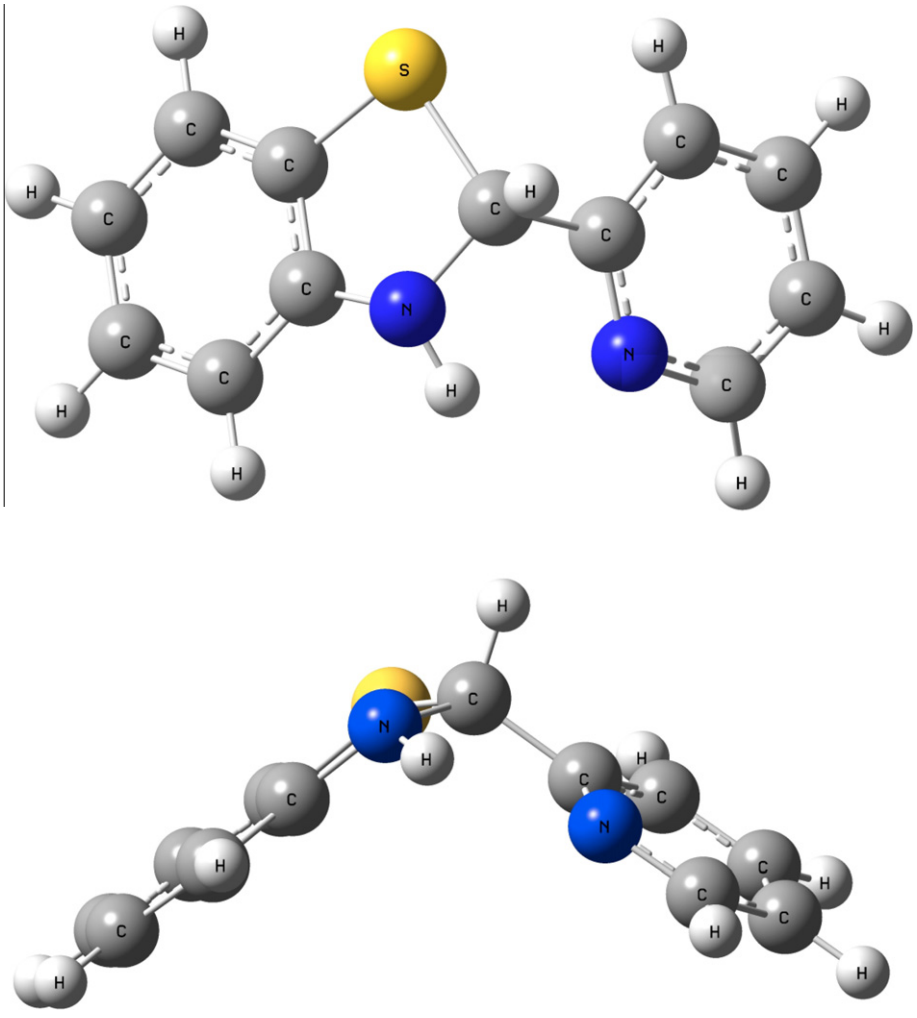

Fig. 9. Two perspectives of the DFT-optimized structure of Py(Bt).

the O_{Fu} atom syn to S_{oBt}. As for Th(oBt) and Pyr(oBt), the lower energy structures have the S and N—H units, respectively, syn to N_{oBt}. Although this point will be discussed further shortly, it is important to recognize that for the lower energy R(oBt) conformation, each of these R group heteroatoms (or N—H unit in the case of the pyrrole analog) is located syn to the Bt heteroatom that has a charge of the opposite sign. This finding is presented graphically in electrostatic potential (ESP) plots for the R(oBt) systems. In each of these depictions, the location of the most negative ESP values (as indicated by the strongest red shading) is N_{oBt}. Of particular note are those systems (R = Py and Fu) that have an electronegative N or O atom with red ESP shading located anti to N_{oBt} and the pyrrolyl-substituted system that has a deep blue ESP shading on the electropositive H atom of the N_{Pyr}—H moiety syn to N_{oBt}. These plots can be found in the Supplementary material. Similar results have been reported for pyrrolyl- and other N-based heterocylic systems, including peptides, in which electrostatic interactions (including H-bonding) are possible between adjacent π-conjugated rings and other functional groups [34–37]. Such arguments have also been recently employed to explain structural preferences of substituted pyrans [38] and carbohydrates. [39,40] In the lower energy conformation of Th(oBt), S_{Th} has a charge of +0.31 and is located syn to N_{oBt}, which has a charge of −0.52. As for Fu(oBt), the lower energy structure has O_{Fu} with a charge of −0.44 syn to S_{oBt}, which has a charge of +0.23. Computationally, Remko and coworkers made a similar finding in their examination of a 2-substituted thiazoline and related species [30].

Various optimized structural parameters for all of the R(oBt) systems are provided in Table 6. The bond lengths determined from the crystal structures (shown in parentheses in Table 6) compare well with those from the Gaussian-optimized structures. For those systems for which two conformations are possible, the computed bond lengths are shown for the more stable structure. Examining the calculated changes in bond lengths upon oxidation (also shown in Table 6) shows that all of the bonds to the $C_{Bt/oBt}$ atom become shorter upon oxidation. The largest change occurs for the N—C bond as it shortens approximately 0.16 Å as both the N_{Bt} and C_{Bt} atoms lose a bond to a H atom and gain a π-bonding interaction to each other. The S—C bond shortens by ca. 0.09 Å such that this bond has a similar length (~1.79 Å) across the series of compounds, as discussed previously for the crystal structures. The C_R—$C_{Bt/oBt}$ bond, which bridges the two ring sections of the molecule, shortens by an average of 0.05 Å, exhibits a rather small change despite the change in geometry of the $C_{Bt/oBt}$ atom upon oxidation and the resulting system-wide π conjugation that can be established. Furthermore, the range of C_R—C_{oBt} bond lengths calculated is quite narrow with a spread of only 0.030 Å separating the longest from the shortest while the actual optimized bond length of ca. 1.46 Å is longer than what might be expected (ca. 1.39 Å) for a bond connecting two C atoms that are both trigonal planar. This observation suggests that the C_R—C_{oBt} π bond is weaker than would be expected for a conjugated π bond. Of particular note is the observation that the compounds that oxidize the fastest (i.e., R = Fu, Pyr, and Th) are found to have the shortest optimized C_R—C_{oBt} bond lengths if by only several hundredths of an Ångstrom.

Table 7
Calculated NLMO bond orders for the C_R—C_{oBt} bonds in the various R(oBt) systems. An asterisk (*) indicates the more stable conformation of R(oBt).

R	Conformation	C_R—C_{oBt} NLMO bond order
Ph	Not applicable	1.0554
Py*	N_{py}—S_{oBt} syn	1.0413
Py	N_{py}—N_{oBt} syn	1.0378
CF_3Ph	Not applicable	1.0501
Th*	S_{Th}—N_{oBt} syn	1.0693
Th	S_{Th}—S_{oBt} syn	1.0639
MeOPh	Not applicable	1.0609
Fu*	O_{Fu}—S_{oBt} syn	1.0690
Fu	O_{Fu}—N_{oBt} syn	1.0707
Pyr*	N—H_{Pyr}—N_{oBt} syn	1.0896
Pyr	N—H_{Pyr}—S_{oBt} syn	1.0887

Another way to probe the relative strengths of the C_R—C_{oBt} π bond is through an examination of calculated bond orders. Gaussian provides such information through the Natural Localized Molecular Orbital (NLMO) analysis [41]. The calculated NLMO bond orders for the C_R—C_{oBt} bonds in each of the R(oBt) systems are provided in Table 7 and the NLMO bond orders are shown in Fig. 10 for all of the bonds in Ph(oBt). As can be seen from Table 7, the calculated NLMO bond orders for these systems show an approximate trend of higher bond order for the products of the faster oxidation reactions and yet these values only span a narrow range from 1.04 to 1.09. Perhaps more importantly, these values suggest that the C_R—C_{oBt} bonds for all of these systems are barely stronger than a single bond. Examination of all of the NLMO bond orders provided in Fig. 10 shows that these values are probably an underestimation of the actual bond orders, given that the calculated values for all of the C—H bonds are approximately 0.74 for bonds that would ordinarily be considered to be single bonds with bond orders of 1.00. Yet compared to the bond orders for the other carbon–carbon bonds of Ph(oBt), which range from 1.20 to 1.75, the bond between C_{Ph} and C_{oBt} is the weakest carbon–carbon bond in the molecule. In line with the observation from Table 6 that the slightly shorter C_R—C_{oBt} bond lengths belong to the systems that oxidize faster, the calculated NLMO bond orders are slightly higher for the same compounds. Furthermore, the C_R—C_{oBt} bond order for different conformations of each of the four systems that can give rise to two different conformers are nearly identical, regardless of the way in which the R group rotates. In three cases (R = Py, Th, Pyr), the bond order is higher for the more stable conformation while it is lower for the fourth (R = Fu).

A molecular orbital (MO) examination of the π-type orbitals in Ph(oBt) explains our observation that the carbon–carbon bond that bridges the R and oBt units is relatively weak. Shown in Fig. 11 is an MO diagram for Ph(oBt) in which only the occupied orbitals of π symmetry are depicted. Not shown in this figure are the molecular orbitals of σ symmetry, which are interspersed with those

Table 6
Structural parameters for the most stable Gaussian-optimized ground-state conformations of R(oBt). Values in parentheses indicate the bond length from the crystal structures obtained as part of this study and are provided for comparison to the computed values.

R	S_{oBt}—C_{oBt} (Å)	N_{oBt}—C_{oBt} (Å)	C_{oBt}—C_R (Å)	Calculated change in bond length upon oxidation		
				S_{oBt}—C_{oBt}—S_{Bt}—C_{oBt} (Å)	N_{oBt}—C_{oBt}—N_{Bt}—C_{oBt} (Å)	C_{oBt}—C_R—C_{Bt}—C_R (Å)
Ph	1.792 (1.749)	1.299 (1.297)	1.469 (1.496)	−0.082	−0.165	−0.041
Py	1.778 (1.749)	1.299 (1.303)	1.469 (1.472)	−0.083	−0.164	−0.067
CF_3Ph	1.789	1.299	1.470	−0.084	−0.164	−0.041
Th	1.790	1.300	1.446	−0.090	−0.164	−0.045
MeOPh	1.794	1.299	1.465	−0.083	−0.166	−0.042
Fu	1.785	1.301	1.442	−0.099	−0.161	−0.044
Pyr	1.783	1.305	1.440	−0.103	−0.166	−0.043

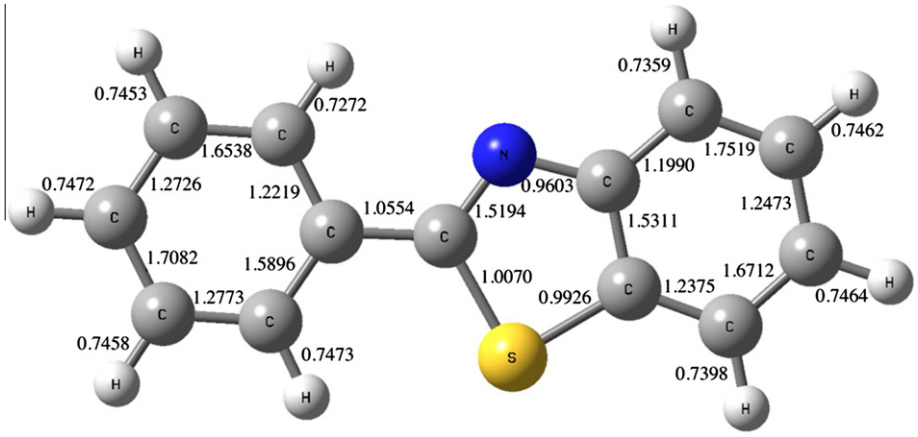

Fig. 10. Calculated NLMO bond orders for all bonds in Ph(oBt).

shown in the diagram. Paired arrows in a given molecular orbital represent the highest occupied orbital for the molecule and molecule fragments; there are no occupied σ-type orbitals that are higher in energy than the highest occupied π-type orbitals. On the left side of the diagram are the three occupied π-type orbitals for the phenyl group shown here as derived from benzene: the completely bonding a_{2u} orbital is below the partially bonding e_g degenerate pair. Although these group theoretical labels are only truly correct for a benzene molecule having D_{6h} symmetry, they shall be used here to differentiate them from the other fragment and molecular orbitals shown in the figure. As for the oBt unit on the right, there are five fragment orbitals that are electronically occupied, ranging from entirely π-bonding across the system at the bottom of the figure, to fragment orbitals with one node in the middle of the diagram, to fragment orbitals with two nodes at the top of the figure.

Together, the three fragment orbitals of the phenyl group and five fragment orbitals of the Bt unit combine to create eight occupied π-type molecular orbitals, shown in the middle of the figure, for Ph(oBt). Molecular orbitals 1a″, 2a″, and 3a″ (group theoretical labels are for the C_s point group) are formed through the combination of the a_{2u} phenyl fragment orbital with the two most stable oBt fragment orbitals (i.e., oBt orbitals 1a″ and 2a″). MOs 1a″ and 2a″ have C_{Ph}—C_{oBt} π bonding character, although this character is predominantly within the Ph and oBt fragments rather than across the bridging carbon atoms, while MO 3a″ does not have C_{Ph}—C_{oBt} π bonding character. MOs 4a″, 6a″, and 7a″ are nonbonding orbitals and contain either Ph or oBt character owing to the fact that each MO is derived from a fragment orbital that has a node that passes through C_{Ph} or C_{oBt}. MOs 5a″ and 8a″ are the C_{Ph}—C_{oBt} π and π* combinations of one of the phenyl e_g orbitals and the second-highest oBt fragment orbital. The occupied C_{Ph}—C_{oBt} π* antibonding orbital (8a″) effectively cancels out the C_{Ph}—C_{oBt} π bonding component (5a″), leaving a weak bridging π bond that owes its strength primarily to the π character from MOs 1a″ and 2a″.

To understand the effect that the electronic occupation of Ph(oBt) molecular orbital 8a″ has on the system, a geometry optimization was performed on a system that has two fewer electrons. Although removing two electrons from Ph(oBt) to generate the dication is one way to do so, it seems more reasonable to use a neutral molecule to eliminate the effect that a 2+ charge would have on the system. Therefore, another way to reduce the number of π-type electrons by two is to replace the S_{oBt} atom with N and to replace the phenyl group with a cyclopentadienyl. Upon undergoing a geometry optimization, this molecule was found to have a bridging C—C bond length of 1.37 Å and a calculated NLMO bond order of 1.69 while the same parameters for Ph(oBt) are 1.47 Å and 1.06, respectively. Therefore, for the R(oBt) systems, occupation of orbital 8a″ with its π* character across the bridging carbon atoms significantly reduces the C_R—C_{oBt} bonding character as compared to a molecule for which this molecular orbital is not occupied.

To summarize, there seem to be two electronic factors, one major and one minor, that contribute to the relative rates of oxidation that are observed experimentally: an electrostatic attraction between heteroatoms in the R and Bt/oBt fragments and some minor influence from the establishment of system-wide π conjugation upon oxidation. With the exception of the pyridinyl-substituted system, the compounds that have heterocyclic R groups oxidize faster than those that possess substituted phenyl groups. The more stable structure for the benzothiazole places the R-group heteroatom on the same side of the molecule as the oppositely charged heteroatom of the oBt fragment. As for π conjugation, the C_R—C_{oBt} bonds are relatively weak as judged by calculated bond orders as well as by the bond lengths determined by geometry optimizations. Such weakness is explained through a molecular orbital treatment of these systems, which shows that the MOs that contain bridging C—C bond π-bonding character are essentially balanced in number by those that possess π* antibonding character.

Given these computational observations, it would be helpful to devise a straightforward method that probes how only these two factors in tandem affect the energetics of this molecular system. One way to do so is by determining the energy difference between a planar R(oBt) structure and a corresponding R(oBt) molecule in which the plane of the R group is perpendicular to that of the oBt fragment. In this manner, the bridging C atoms maintain their trigonal planarity. The effect of the establishment of a conjugated π system on the C_R—C_{oBt} bond length can be examined as the R and oBt rings are fixed in orientations in which their individual π systems are either orthogonal (i.e., no π bonding allowed between the two fragments) or co-planar with each other. All other bond lengths and angles were allowed to optimize. Table 8 summarizes the results of these calculations. It is important to emphasize that simply rotating the R group from perpendicular to coplanar with the oBt unit is meant to be a means of gauging how much each R(oBt) system is stabilized by the coplanarity of the R and oBt fragments and is not meant to be a representation of the oxidation reaction itself.

What is particularly remarkable about the data shown in Table 8 is that, with the exception of the values for the two Py(oBt) conformers, the molecules that have larger energies of stabilization are those for which have a greater propensity to undergo oxidation, especially when the values that correspond to the more stable conformer for the heteroatom-containing R group systems are

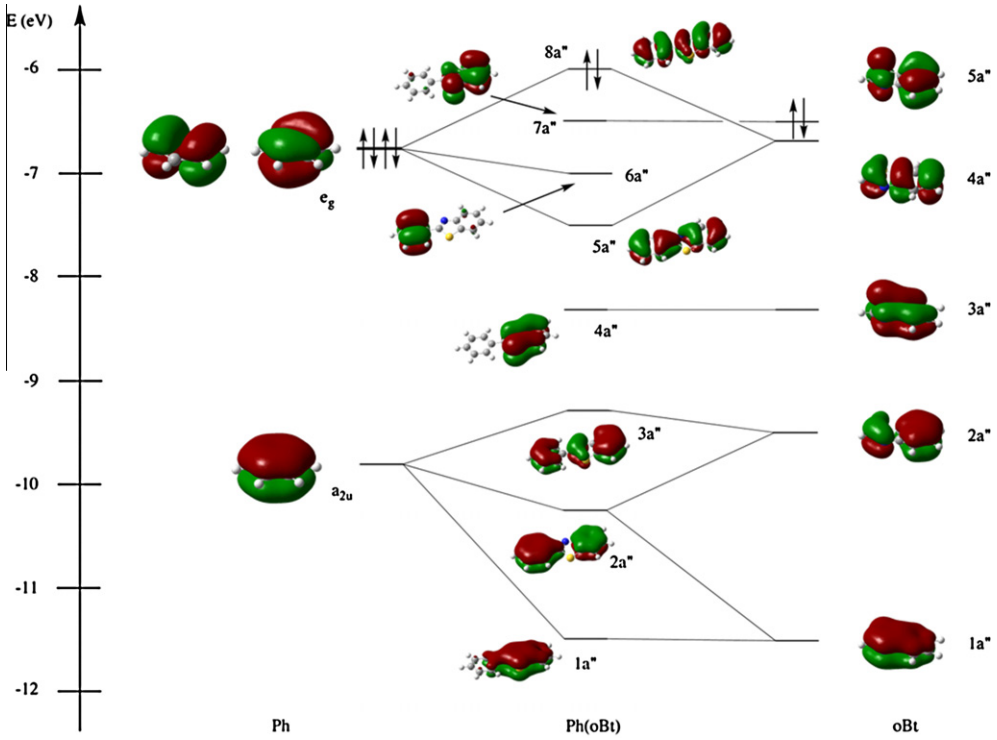

Fig. 11. Molecular orbital diagram of the π-type orbitals of Ph(oBt).

considered. Remembering that these values are only comparisons of the differences in total energies between R(oBt) structures in which the R and oBt fragments are either coplanar, these energies take into account not only the stabilization gained from the formation of a system-wide conjugated π system but also the energy that results from the interaction of the heteroatoms on the R and oBt groups. For Th(oBt), Fu(oBt), and Pyr(oBt), which are the products of the faster oxidation reactions, the energies of stabilization range from 6.50 kcal/mol to 9.47 kcal/mol when the R group is rotated into the orientation having a more favorable electrostatic interaction or from 5.04 kcal/mol to 6.01 kcal/mol when rotated to the less favorable configuration. For the R(oBt) systems in which the R group does not contain a heteroatom within the ring (i.e., R = Ph, CF_3Ph, MeOPh), the span of energies of stabilization from 5.31 to 5.79 kcal/mol is narrower and the values themselves are smaller in magnitude than for Th(oBt), Fu(oBt), and Pyr(oBt). Thus, rotating the R group into the more favorable orientation imparts a larger energy of stabilization upon those compounds with a heterocyclic R group than for any of the systems with a phenyl R group. Of course, the one compound for which the calculated energy of stabilization does not correlate with the experimental relative rate of reaction is the pyridinyl-substituted species. The energy determined for this molecule is the second highest of the entire series, which means that this compound would be expected to have one of the fastest oxidation rates. As will be summarized shortly, this system must have some other effect that causes the oxidation reaction to be the slowest of the compounds that we have examined here.

Despite the nearly doubling of the energy of stabilization from the phenyl analog to the pyrrolyl-substituted system, as can be seen in Table 9 there is little change in the C_R—C_{oBt} bond lengths either between the perpendicular and coplanar conformations of a given R(oBt) system or for this difference across the entire span of molecules. Further evidence of the relatively weak π bonding in the C_R—C_{oBt} bond is the small decrease in bond length (no more than 0.029 Å) as each R(oBt) system is allowed to convert from a perpendicular conformation to parallel. In line with previous comments here regarding the C_R—C_{oBt} bond lengths, the compounds that oxidize the fastest exhibit the largest decrease in this distance as well as the shortest C_R—C_{oBt} bond lengths as shown in Table 9. The C—C bond length shortens the most for Pyr(oBt) (−0.029 Å) and for Fu(oBt) (−0.026 Å), which are the products of the fastest oxidation reactions, but the magnitude across the entire span of molecules (0.016–0.029 Å) is quite small. This finding confirms that the heteroatom-induced electrostatic interactions between the R and oBt fragments are indeed the primary reason for this effect.

The most immediate question that arises from the computational results pertains to the particular order of observed relative rates of reaction and why there seems to be a discrepancy for the pyridinyl-substituted analog. Given the factors discussed above, it seems best to separate these seven compounds into three separate classes: (1) systems with R groups that possess either a non-N heteroatom (R = Fu and Th) or that have a nitrogen that does not have a lone pair that is capable of having an electrostatic interaction with the H atom on N_{Bt} (R = Pyr), (2) systems with R groups that do not possess a heteroatom in the ring (R = Ph, CF_3Ph, MeOPh), and (3) the system that has an R group possessing a nitrogen atom that does have an electron lone pair that can interact with the N_{Bt} H atom (R = Py).

The first group of molecules contains R groups that have heteroatoms in the ring: Pyr, Fu, and Th. For these three systems, there is a definite energy preference for the direction in which the R group prefers to be oriented in the oxidized compound. As can be seen in Table 7, these molecules are calculated to have slightly shorter C_R—C_{oBt} bonds but the primary structural influence is that each can establish favorable electrostatic interactions between the charges on the heteroatoms of the R and oBt fragments.

The second group of molecules contains R groups that do not have heteroatoms in the ring: Ph(Bt), CF_3Ph(Bt), and MeOPh(Bt). For these three systems, there is no energy preference regarding the direction in which the R group rotates to become coplanar with

Table 8
Energy of stabilization obtained when geometry of R(oBt) system is converted from perpendicular to planar.

R	Energy of stabilization to more stable R(oBt) conformer (kcal/mol)	Energy of stabilization to less stable R(oBt) conformer (kcal/mol)
Ph	5.31	
Py	9.32	2.60
CF_3Ph	5.39	
Th	6.50	5.04
MeOPh	5.79	
Fu	7.67	5.51
Pyr	9.47	6.01

Table 9
Optimized C_R—C_{oBt} bond lengths for perpendicular and coplanar R(oBt) systems.

R	C_R—C_{oBt} bond length (Å)		Change
	Perpendicular	Coplanar	
Ph	1.485	1.469	−0.016
Py	1.492	1.469	−0.023
CF_3Ph	1.486	1.470	−0.016
Th	1.471	1.446	−0.025
MeOPh	1.483	1.465	−0.018
Fu	1.468	1.442	−0.026
Pyr	1.469	1.440	−0.029

oBt upon oxidation because none of these systems have a heteroatom in R that can become syn to an oppositely charged heteroatom in the oBt portion of the molecule. Given the results in Table 8 in which the energies of stabilization for Ph(oBt) and CF_3Ph(oBt) are essentially the same while that for MeOPh(oBt) is approximately 0.40 kcal/mol greater, a very slight difference in C_R—C_{oBt} π bonding owing to the presence and nature of a substituent on the phenyl ring appears to be the only factor responsible for the difference in the relative rates of reaction of each of these R(Bt) systems. Among these three systems, as shown in Table 9, CF_3Ph(oBt) does have the highest C_R—C_{oBt} bond order albeit by only 0.005 units more than MeOPh(oBt) when the R and oBt groups are coplanar.

The final molecule, the pyridinyl-substituted system, appears to be a special case of the electronic factors discussed above. While it does indeed have a heteroatom-containing R group, which would at first suggest that it should undergo oxidation among the fastest of the systems examined here as evidenced by the energy of stabilization presented in Table 8, the relatively low C_{Py}—C_{oBt} bond order given in Table 7 and the orientation of the pyridinyl ring in the structure of Py(Bt) that is different than for the R groups in all of the other benzothiazolines indicate otherwise. While we have more work to flesh out the mechanism of this oxidation reaction, we suspect that it is this electrostatic interaction between N_{Py} and the H atom of N_{Bt} that acts to impede the loss of this H atom from the molecule, thereby slowing the oxidation reaction.

4. Conclusions

This work presents a discussion of the ground-state factors that influence the relative rates of oxidation for a set of 2-benzothiazoline analogs. We find that, with one exception, benzothiazolines that possess a heterocyclic R group oxidize faster than those with a phenyl group. Although one would expect that the establishment of π conjugation across the C_R—C_{oBt} bond would be a driving force in the reaction, our computations suggest that the establishment of a favorable electrostatic interaction between the heteroatoms of the R and Bt/oBt fragments is the primary influence on this reaction.

Acknowledgments

This work was supported by an NTID Faculty Evaluation and Development Grant (MAL) as well as generous financial support from Union College (LAT). We also thank the National Science Foundation (NSF 0521237) for supporting the X-ray diffraction facility at Vassar College (JMT).

Appendix A. Supplementary material

CCDC 808288, 809123, 808557 and 809122 contain the supplementary crystallographic data for Ph(Bt), Py(Bt), Ph(oBt) and Py(oBt) respectively. These data can be obtained free of charge from The Cambridge Crystallographic Data Centre via www.ccdc.cam.ac.uk/data_request/cif. Supplementary data associated with this article can be found, in the online version, at doi:10.1016/j.molstruc.2011.12.001.

References

[1] J.C. Kwan, R. Ratnayake, K.A. Abboud, V.J. Paul, H. Luesch, J. Org. Chem. 75 (2010) 8012.
[2] S. Zhang, R. Pattacini, P. Braunstein, Organometallics 29 (2010) 6660.
[3] L.J. Carlson, J. Welby, K.A. Zebrowski, M.M. Wilk, R. Giroux, N. Ciancio, J.M. Tanski, A. Bradley, L.A. Tyler, Inorg. Chim. Acta 365 (2011) 159.
[4] S. Fustero, E. Salavert, A. Navarro, F. Mojarrad, A.S. Fuentes, in: O.A. Attanasi, D. Spinelli, (Eds.), Targets in Heterocyclic Systems, vol. 5, Italian Society of Chemistry, 2001, pp. 235–270.
[5] A.C. Gaumont, M. Gulea, J. Levillain, Chem. Rev. 109 (2009) 1371.
[6] L.A. Tyler, M.M. Olmstead, P.K. Mascharak, Inorg. Chem. 42 (2001) 5408.
[7] R. Pattacini, G. Margraf, A. Messaoudi, N. Oberbeckmann-Winter, P. Braunstein, Inorg. Chem. 21 (2008) 9886.
[8] S.F. Lu, D.M. Du, J. Xu, S.W. Zhang, J. Am. Chem. Soc. 128 (2006) 7418.
[9] L.F. Lindoy, Coord. Chem. Rev. 4 (1969) 41.
[10] M. Akbar Ali, S.E. Livingstone, Coord. Chem. Rev. 13 (1974) 101.
[11] H.A. Tayim, A.S. Salameh, Polyhedron 2 (1983) 1091.
[12] K. Singh, R. Singh, J.P. Tandon, Bull. Chem. Soc. Jpn. 61 (1988) 4494.
[13] K.S. Ramasamy, R. Bandaru, D. Averett, J. Org. Chem. 65 (2000) 5849.
[14] D.R. Williams, P.D. Lowder, Y.G. Gu, D.A. Brooks, Tetrahedron Lett. 38 (1997) 331.
[15] V.C. Ezeh, A.K. Patra, T.C. Harrop, Inorg. Chem. 49 (2010) 2586.
[16] Y. Huang, H. Gan, S. Li, J. Xu, X. Wu, H. Yao, Tetrahedron 51 (2010) 1751.
[17] T. Itoh, K. Nagata, H. Ishikawa, A. Ohsawa, Heterocycles 63 (2004) 2769.
[18] C.J. Jones, J.A. McCleverty, J. Chem. Soc. A 12 (1971) 37.
[19] A.S. Salameh, H.A. Tayim, B.C. Uff, Polyhedron 6 (1982) 543.
[20] A.C. Braithwaite, C.E.F. Rickard, T.N. Waters, Inorg. Chim. Acta 26 (1978) 63.
[21] A.C. Braithwaite, C.E.F. Rickard, T.N. Waters, Transition Met. Chem. 1 (1975) 5.
[22] G. M Sheldrick, Acta Cryst. A 64 (2008) 112.
[23] M.J. Frisch, G.W. Trucks, H.B. Schlegel, G.E. Scuseria, M.A. Robb, J.R. Cheeseman, J.A. Montgomery Jr., T. Vreven, K.N. Kudin, J.C. Burant, J.M. Millam, S.S. Iyengar, J. Tomasi, V. Barone, B. Mennucci, M. Cossi, G. Scalmani, N. Rega, G.A. Petersson, H. Nakatsuji, M. Hada, M. Ehara, K. Toyota, R. Fukuda, J. Hasegawa, M. Ishida, T. Nakajima, Y. Honda, O. Kitao, H. Nakai, M. Klene, X. Li, J.E. Knox, H.P. Hratchian, J.B. Cross, V. Bakken, C. Adamo, J. Jaramillo, R. Gomperts, R.E. Stratmann, O. Yazyev, A.J. Austin, R. Cammi, C. Pomelli, J.W. Ochterski, P.Y. Ayala, K. Morokuma, G.A. Voth, P. Salvador, J.J. Dannenberg, V.G. Zakrzewski, S. Dapprich, A.D. Daniels, M.C. Strain, O. Farkas, D.K. Malick, A.D. Rabuck, K. Raghavachari, J.B. Foresman, J.V. Ortiz, Q. Cui, A.G. Baboul, S. Clifford, J. Cioslowski, B.B. Stefanov, G. Liu, A. Liashenko, P. Piskorz, I. Komaromi, R.L. Martin, D.J. Fox, T. Keith, M.A. Al-Laham, C.Y. Peng, A. Nanayakkara, M. Challacombe, P.M.W. Gill, B. Johnson, W. Chen, M.W. Wong, C. Gonzalez, J.A. Pople, Gaussian 03, Revision E.01, Gaussian, Inc., Wallingford, CT, 2004.
[24] A.D. Becke, J. Chem. Phys. 78 (1993) 5648.
[25] C. Lee, W. Yang, R.G. Parr, Phys. Rev. B 37 (1988) 785.
[26] S.F. Soua, P.A. Fernandes, M.J. Ramos, J. Phys. Chem. A 111 (2007) 10439.
[27] H.P. Lankelma, P.X. Sharnoff, J. Am. Chem. Soc. 53 (1931) 2654.
[28] K. Yamamoto, M. Fujita, K. Tabashi, Y. Kawashima, E. Kato, M. Oya, T. Iso, J. Iwao, J. Med. Chem. 31 (1988) 919.
[29] M. Hori, T. Kataoka, J. Shimizu, Y. Imái, Chem. Pharm. Bull. 27 (1979) 1982.
[30] M. Remko, O.A. Walsh, W.G. Richards, Chem. Phys. Lett. 336 (2001) 156.
[31] M. Remko, P.T. Van Duijnen, M. Swart, Chem. Struct. 14 (2003) 271.
[32] J. Chowdhury, J. Sarkar, T. Tanaka, G.B. Talapatra, J. Phys. Chem. C 112 (2008) 227.
[33] S. Abdalla, M. Springborg, J. Phys. Chem. A 114 (2010) 5823.
[34] A. Tabatchnik, V. Blot, M. Pipelier, D. Dubreuil, E. Renault, J.Y. Le Questel, J. Phys. Chem. A 114 (2010) 6413.

[35] A. Tabatchnik-Rebillon, C. Aubé, H. Bakkali, T. Delaunay, G.T. Manh, V. Blot, C. Thobie-Gautier, E. Renault, M. Soulard, A. Planchat, J.Y. Le Questel, R. Le Guével, C. Guguen-Guillouzo, B. Kauffmann, Y. Ferrand, I. Huc, K. Urgin, S. Condon, E. Léonel, M. Evain, J. Lebreton, D. Jacquemin, M. Pipelier, D. Dubreuil, Chem. Eur. J. 16 (2010) 11876.
[36] Y.K. Kang, B.J. Byun, J. Phys. Chem. B 111 (2007) 5377.
[37] R. Hilal, Z.M. Zaky, S.A.K. Elroby, J. Mol. Struct.-Theochem. 685 (2004) 35.
[38] Y. Mo, Nat. Chem. 2 (2010) 666.
[39] G. Cuevas, J. Am. Chem. Soc. 122 (2000) 692.
[40] E.J. Cocinero, P. Çarçabal, T.D. Vaden, J.P. Simons, B.G. Davis, Nature 496 (2011) 76.
[41] A.E. Reed, F. Weinhold, J. Chem. Phys. 86 (1985) 1736.